

# Theoretical, experimental and numerical study of lateral buckling in glued laminated timber beams

Guillermo Capellán<sup>a</sup>, Javier Sánchez-Haro<sup>b,\*</sup>, Pablo de Celis<sup>a,b</sup>, Ana B. Ramos-Gavilán<sup>c</sup>

<sup>a</sup> Arenas&Asociados Ingeniería de Diseño S.L., c/ Marqués de la Ensenada 11, Santander 39009, Spain

<sup>b</sup> Department of Structural Engineering, University of Cantabria, Av. de los Castros 44, Santander 39005, Spain

<sup>c</sup> Department of Mechanical Engineering, Universidad de Salamanca, Avda. Requejo, 33, Zamora 49022, Spain

## ARTICLE INFO

### Keywords:

Glued laminated timber  
Structural stability  
Lateral buckling  
Experimental tests  
Nonlinear analysis

## ABSTRACT

There is an upward trend in the use of glued laminated timber in increasingly slender structures, which requires special attention to instability effects, such as lateral buckling. This article presents the results of lateral buckling loads from an experimental campaign focusing on specimens with a relative slenderness greater than 1.4 (elastic range) and involving a total of 14 beams – 10 with constant depth and 4 with variable depth. These results are then compared with those obtained using the Eurocode, which does not account for the influence of knots and fiber deviation, and a numerical finite element model for validation. All tested beams exhibited an initial misalignment within the tolerances allowed by the Eurocode to analyze its influence. For the testing campaign, a novel loading system was designed, enabling more precise experimental results. From the results, the initial misalignment value was correlated with the loss of lateral buckling load capacity due to the stress exhaustion caused by the transverse displacement of the beam prior to instability. The article proposes a modification to the Eurocode formulation for calculating the critical lateral buckling load, incorporating this effect for slenderness within the elastic range.

## 1. Introduction

Current trends in construction, driven by extraordinary technical advancements and economic demands, have led to the development of structural designs that must maximize strength and lightness while adhering to the safety standards established by regulations. These requirements have resulted in a continuous increase in the slenderness and lightness of load-bearing structural elements. Consequently, accounting for instability and second-order effects has become a crucial factor in their design and sizing. In this context, glued laminated timber (GLU-LAM) is gaining ground over metallic elements due to its lightness and strength, performing well in bending and compression at an acceptable cost while also offering aesthetic and sustainability advantages. The optimal design of GLULAM structural elements leads to slender cross-sections with a high height-to-width ratio, ensuring good bending performance in the vertical plane and stiffness against deformations but with very low inertia in the transverse direction. This latter characteristic makes structures of this material susceptible to transverse instability or lateral buckling, which significantly reduces their bending strength. The European timber standard EC5 [1] provides specific formulas for checking lateral torsional buckling in straight beams with

constant cross-sections (other geometries, such as variable cross-sections or curved shapes, are not considered). These formulas are derived from linear stability theory (second-order linear) for high slenderness ratios and from an estimation based on strength and slenderness for intermediate slenderness ratios. These verifications are calibrated for an idealized member and do not consider key characteristic of timber, such as fiber deviation, knots, etc. They also overlook real-world structural conditions like load eccentricities or geometric imperfections, although EC5 [1] does introduce a straightness deviation limit of  $L/500$ . There is, therefore, a regulatory gap compared to steel, despite its homogeneous nature. In EC3 [2] imperfections are considered in buckling and lateral-torsional buckling resistance through buckling curves or lateral-torsional buckling curves, respectively. What EC5 [1] does consider is the variability of the material, by taking as characteristic values of its properties ( $E_k$  and  $G_k$ ) those associated with the 5% percentile (in the same way as EC3 [2] does for steel). This guarantees a certain safety margin, together with the use of partial safety coefficients, used in the calculation of the design resistances.

The formulation proposed by EC5 [1] for checking lateral buckling in timber originates from the studies of Hooley & Madsen [3]. They validated Timoshenko's theory [4] for an ideal beam and applied it GLU-LAM, a heterogeneous and anisotropic material, in a manner analogous

\* Corresponding author.

<https://doi.org/10.1016/j.engstruct.2025.120558>

Received 15 December 2024; Received in revised form 22 April 2025; Accepted 12 May 2025

Available online 21 May 2025

0141-0296/© 2025 The Author(s). Published by Elsevier Ltd. This is an open access article under the CC BY license (<http://creativecommons.org/licenses/by/4.0/>).

**Symbols used**

$E$	Modulus of elasticity parallel to the fiber	$P_{cr}$	Critical lateral buckling load (collapse failure due to instability)
$E_k$	Characteristic value of the elasticity modulus parallel to the fiber	$P_{cu}$	Asymptotic value of the load in the load-stress graph of the tests
$E_{mean}$	Mean value of the elasticity modulus parallel to the fiber	$P_u$	Ultimate load (collapse failure due to bending)
$E_r$	Value of the elasticity modulus parallel to the fiber obtained indirectly from the tests through the Eurocode	$R_k$	Characteristic strength
$f$	Function of a serie of parameters	$W_y$	Section modulus about the strong axis
$G$	Shear modulus parallel to the fiber	$b$	Cross-section width of the beam
$G_k$	Characteristic value of the shear modulus parallel to the fiber	$h$	Cross-section height of the beam
$I_t$	Torsional moment of inertia	$f_{m,k}$	Characteristic bending strength
$I_z$	Second moment of area about the weak axis	$k_{crit}$	Factor reducing flexural strength due to lateral buckling
$L$	Real length of the beam	$\lambda_{rel}$	Relative slenderness ratio of the beam
$L_{ef}$	Effective length of the beam	$\rho$	Density
$M_{cr}$	Elastic critical lateral buckling bending moment (instability failure)	$\sigma_{cr}$	Critical lateral buckling stress (collapse failure due to instability)
$M_u$	Elastic ultimate bending moment (bending failure)	$\sigma_u$	Ultimate stress (collapse failure due to bending)
$P_{f_{m,k}}$	Load for which the characteristic bending stress is reached	$\omega$	Factor reducing load resistant to lateral buckling due to nonlinear effects

to Euler's studies [5] on column buckling. However, although Hooley & Madsen's [3] study pertains to glued laminated timber beams, the specimens tested at the time were planks of clear, dry Douglas fir, meaning sawn timber pieces. Furthermore, as the wood was clear, there were no knots, although in one of the specimens tested, knots were simulated by mechanically drilled holes. This methodology raises certain questions regarding its validity, as a hole may simulate a discontinuity in the fiber similar to that caused by a knot but does not replicate the fiber deviation produced by a knot. In any case, material imperfections are not considered in the formulation proposed in that study, nor in EC5 [11]. In the test used by Hooley & Madsen [3] in 1964 (Fig. 1), as well as in other more recent investigations, such as those by Trahair (1996) [6] (Fig. 2) or Xiao (2017) [7] (Fig. 3), the load was applied using dead weights suspended by supports attached to the beams under study.

This method of load application ensures the total verticality of the force and the absence of horizontal forces at the top of the beams throughout the lateral displacement process experienced by the beam during loading. However, it imposes a maximum applicable load, which limits the study of larger beams.

Another consequence of applying the load in this manner is its discrete, stepwise nature, which means that the results obtained are also non-continuous. Additionally, this approach may lead to dynamic or asymmetry effects during the loading process, causing sudden lateral displacements due to the high sensitivity of the beam near the instability load.

Consequently, an advancement over the previous load application systems is the test devised by Larsen [8], which applies the load through a system of rods. One end of the rods is secured, and they pull on the

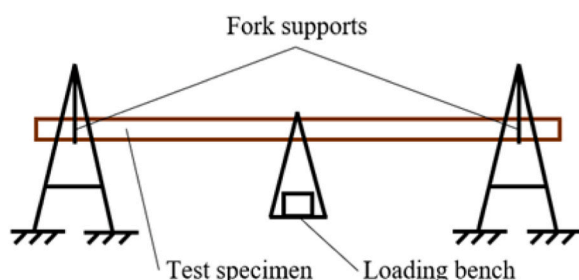


Fig. 1. Hooley & Madsen test on clear Douglas fir wood beams [3].

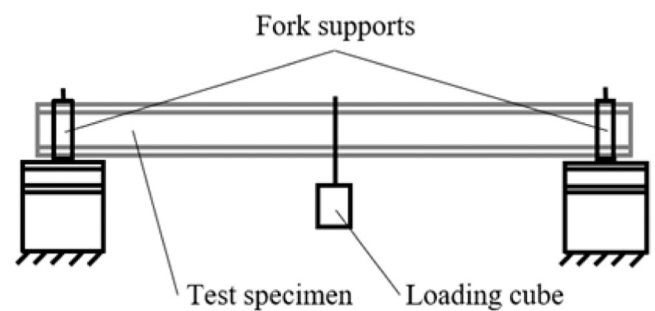


Fig. 2. Trahair test on beams based on steel profiles [6].



Fig. 3. Xiao test on lumber joists (glued laminated timber) [7].

beams when a hydraulic press, located between two beams connected to the rods at their other ends, is activated. Unlike the earlier systems that applied the load only at the mid-span, Larsen's system [8] distributed the bending loads at the thirds of the beam, creating two points of application. Additionally, it is introduced an axial compression load through another hydraulic press located at one end of the beam. This system allows for the continuous, step-free application of the load, although it does not fully guarantee its correct direction. Furthermore, since the beam under test is placed vertically, as shown in Fig. 4, the self-weight does not influence the instability phenomenon.

Recently, Töpler & Kuhlmann [9,10] (Fig. 5) and Wilden, Hoffmeister & Feldmann [11,12] (Fig. 6) have each conducted experimental, theoretical, and numerical research on lateral buckling in glued laminated timber beams, considering their initial imperfections and

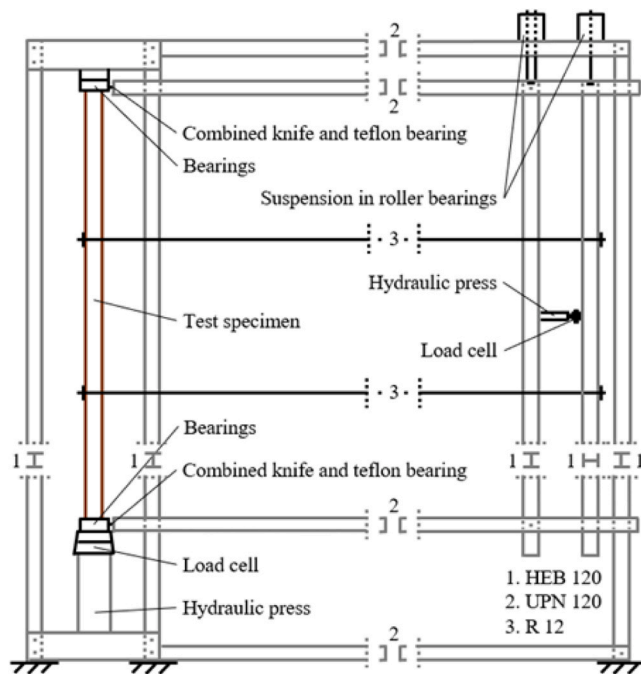


Fig. 4. Larsen test on sawn redwood beams [8].

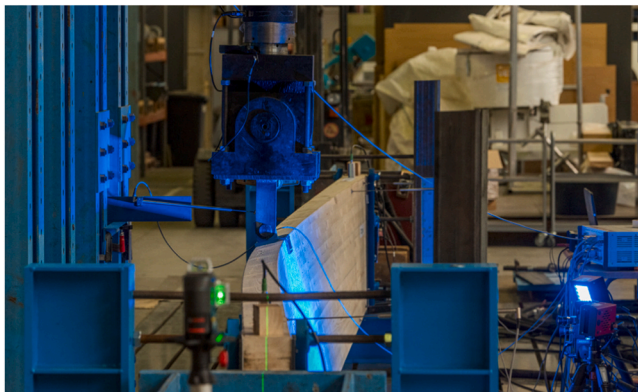


Fig. 5. Töpler & Kuhlmann test on glued laminated timber [9].

nonlinear effects. For their respective experimental studies, they designed a continuous loading system using a hydraulic cylinder that ensures the load remains vertical as the beam deforms horizontally, enabling continuous data recording. However, this approach introduces the drawback of applying a horizontal force at the top of the beams when lateral displacement occurs – a force that did not appear in earlier mechanical tests [3,6,7]. This horizontal force, due to the torsional moment it generates and its partial compensation of lateral instability, can have a significant influence on the results. Additionally, both studies have focused on the analysis of beams in the inelastic range, unlike the present research, in which nine out of the ten tested beams with constant depth fall within the elastic range (along with four tested beams with variable depth), where lateral buckling is more significant.

Other interesting lines of research in the field of lateral buckling in timber involve the types of beam supports. These include proposals to improve adjustments for calculating the effective length in simply supported beams and cantilevers [7], as well as studies on the difference in strength between ideal supports and commercial supports and connections used in construction [13]. Besides, several investigations have analyzed, through second-order analyses, the influence of initial imperfections on lateral buckling resistance when, in addition to bending



Fig. 6. Wilden, Hoffmeister & Feldmann test on glued laminated timber [12].

loads, there is an axial compression load [14–16]. These studies propose treating such situations as a holistic phenomenon, rather than addressing the forces separately, as currently stipulated in EC5 [1]. It is worth mentioning the studies conducted in recent years on the lateral stability of composite timber beams, both with rectangular cross-sections [17], as well as "T"-shaped beams [13,18,19] or those with corrugated webs [20]. Finally, it is also noteworthy to highlight some publications on how high temperatures affect the lateral instability of beams [21,22].

The objective of this article is to provide design engineers with greater certainty when making design considerations regarding the lateral buckling of wood. This is achieved through an experimental study that addresses three key aspects. First, it develops a novel testing method for the lateral buckling of beams, achieving greater accuracy in experimental results for comparison with theoretical predictions. Second, the article aims to demonstrate the influence of knots and fiber deviations in wood on experimental results and to highlight the need for these effects to be accounted for in regulations. Finally, the article proposes incorporating the influence of second-order nonlinearity into the lateral buckling formulation in wood, as defined by EC5 [1], through a coefficient based on the value of the initial imperfection.

This article is structured as follows: it begins with the *Introduction* section, which contextualizes the problem and highlights the limitations of the current formulation proposed by EC5 [1] for verifying lateral buckling in timber elements. Next, the *Methodology* section provides a detailed description of the EC5 [1] formulation for lateral buckling. Moreover, the experimental testing campaign is explained and the numerical analysis performed using the finite element method (FEM) is described in detail. This is followed by the *Results Comparison* section, where the results obtained through the three methodologies are presented and compared. Subsequently, the *Discussion of the Results* section comments on and compares the various findings. Finally, the main conclusions drawn from the research are presented in the *Conclusions* section.

## 2. Methodology

The objective of this section is to present the analysis conducted on GLULAM timber beams regarding lateral buckling, based on the EC5 [1] standard, through the experimental testing campaign and the numerical finite element analysis.

## 2.1. EC5 lateral buckling formulation review

The provisions of EC5 [1] define a cross-sectional criterion whereby the stresses in a fiber must not exceed the characteristic bending strength ( $f_{m,k}$ ) of the timber under study, both in terms of bending and instability. This implies compliance with the following inequalities:

$$\sigma_u \leq f_{m,k} \text{ 1st order (bending)}$$

$$\sigma_{cr} \leq k_{crit} f_{m,k} \text{ 2nd order (instability)}$$

These limit stresses for bending ( $\sigma_u$ ) and instability ( $\sigma_{cr}$ ) define the characteristic strength ( $R_k$ ) of the cross-section. They establish the failure criterion associated with their respective loads,  $P_u$  and  $P_{cr}$ , or maximum moments  $M_u$  and  $M_{cr}$ , which depend on the position and type of applied load.

$$\sigma_u = \frac{M_u}{W_y} = \frac{f(P_u, L)}{W_y} \leq f_{m,k} \quad \sigma_{cr} = \frac{M_{cr}}{W_y} = \frac{f(P_{cr}, L)}{W_y} \leq k_{crit} f_{m,k}$$

Regarding the critical condition, as noted in [23], the expressions for calculating  $M_{cr}$  or  $\sigma_{cr}$  are derived from the classical formulation of lateral buckling. This formulation assumes that instability occurs due to bending about the weak axis and neglects the influence of warping caused by non-uniform torsion, a negligible phenomenon in narrow rectangular sections. This classical formulation is presented below:

$$M_{cr} = \frac{\pi}{L_{ef}} \sqrt{EI_z GI_t} \quad \sigma_{cr} = \frac{\pi}{L_{ef} W_y} \sqrt{EI_z GI_t}$$

Given that the material is timber and the sections are the commonly used rectangular ones, the following two assumptions can be made regarding the torsional inertia ( $I_t$ ) and the shear modulus ( $G_k$ ):

$$I_t = \frac{hb^3}{3} \left(1 - 0.63 \frac{b}{h}\right) \approx \frac{hb^3}{3} \quad G_k \approx \frac{E_k}{16}$$

Additionally, the well-known expressions for the moment of inertia about the weak axis ( $I_z$ ) and the section modulus with respect to the strong axis ( $W_y$ ), considering a rectangular section, are:

$$I_z = \frac{hb^3}{12} \quad W_y = \frac{bh^2}{6}$$

By applying these expressions and simplifications to the formulas of the classical theory presented earlier, the following simplified expressions are obtained. These are the ones established by EC5 [1] for calculating timber beams with rectangular cross-sections:

$$M_{cr} = \frac{0.13b^3 h}{L_{ef}} E_k \quad \sigma_{cr} = \frac{0.78b^2}{h L_{ef}} E_k$$

Specifically, for the case being studied in this article, that is, a point load at the mid-span of the beams, the expression that allows the calculation of the critical load is the one deduced below:

$$P_{cr} = M_{cr} \frac{4}{L} = \sigma_{cr} W_y \frac{4}{L} = k_{crit} f_{m,k} \frac{bh^2}{6} \frac{4}{L} = \frac{k_{crit} f_{m,k} bh^2}{1.5L}$$

The factor  $k_{crit}$  takes into account the reduction in bending strength due to lateral buckling. Its value is defined in EC5 [1] for each range of lateral buckling – bending, inelastic and elastic (Fig. 37) – based on an expression dependent on the relative bending slenderness.

$$\lambda_{rel} = \sqrt{\frac{f_{m,k}}{\sigma_{cr}}} = \sqrt{\frac{h L_{ef}}{0.78b^2} \frac{f_{m,k}}{E_k}}$$

$$k_{crit} = 1 \text{ for } \lambda_{rel} \leq 0.75 \text{ (bending range)}$$

$$k_{crit} = 1.56 - 0.75\lambda_{rel} \text{ for } 0.75 < \lambda_{rel} \leq 1.4 \text{ (inelastic range)}$$

$$k_{crit} = 1/\lambda_{rel}^2 \text{ for } 1.4 < \lambda_{rel} \text{ (elastic range)}$$

It is important to note that the inelastic range is approximated, as indicated, by a straight line, which connects the elastic range with the ordinary bending range. Due to this approximation, it is the area with the greatest difference between the normative results and the experimental behavior.

By substituting the respective value of  $k_{crit}$  in the expression that allows obtaining the critical lateral buckling load, the formulas that provide said load directly based on the geometry and the material parameters ( $f_{m,k}$  and  $E_k$ ) are deduced for the ranges involved in this investigation.

- Inelastic range. Eq. [1]:

$$P_{cr} = 1.56 \frac{f_{m,k} bh^2}{1.5L} - 0.75 \sqrt{\frac{f_{m,k}^3 h^5 L_{ef}}{1.755L^2 E_k}}$$

- Elastic range. Eq. [2]:

$$P_{cr} = \frac{0.52b^3 h}{L L_{ef}} E_k$$

It is worth mentioning that prEN 1995 [24] would abandon the sectional definition of  $k_{crit}$  to propose a continuous curve based on relative slenderness. Furthermore, the project to update the current European regulations provides guidelines for calculations according to the second-order theory, with a unified imperfection value of  $L/1000$  at the centre of the beam.

To consider the influence of support conditions and load configuration, EC5 [1] employs the equivalent beam method. This is based on calculating the critical load for a beam with an effective length ( $L_{ef}$ ), according to Table 1:

All that has been presented in this section, related to the EC5 [1] methodology, is only applicable to beams with constant depth. In the case of verifying beams with variable depth, which are commonly used today, EC5 [1] does not provide any formulation to be applied. In this situation, for this research, the variable depth beams are analyzed using EC5 [1] by considering them as beams with a constant average depth.

## 2.2. Experimental analysis

In this testing campaign, commercial GLULAM pieces were used to consider the influence of the real timber conditions, such as its quality (fiber deviation and knots) and imperfections. The campaign also accounted for manufacturing and installation tolerances, as well as the scale and support and load conditions. The importance of considering these circumstances was detailed by Capellán [25]. The tests consisted of applying a vertical load at the mid-span of various beams with fork-type supports at their ends, until the lateral instability load was reached. The details of the tests are shown below.

### 2.2.1. Description of the analysed beams

For the experimental part of this research, two types of GL-28 specimens (GLULAM with a characteristic bending strength of 28 MPa) were used: beams with constant depth and beams with variable depth. The batch of constant depth beams for testing consisted of 10 specimens, divided into 4 different geometries. As for the beams with variable depth, four specimens with the same geometry were tested the variation between the outer depths being linear.

**Table 1**  
Effective length as a ratio of the span according to EC5 [1].

Beam type	Loading type	$L_{ef}/L^*$
Simply supported	Constant moment	1.0
	Uniformly distributed load	0.9
	Concentrated force at the middle of the span	0.8
Cantilever	Uniformly distributed load	0.5
	Concentrated force at the free end	0.8

\*The ratio between the effective length  $L_{ef}$  and the span  $L$  is valid for a beam with torsionally restrained supports and loaded at the centre of gravity. If the load is applied at the compression edge of the beam,  $L_{ef}$  should be increased by 2 h and may be decreased by 0.5 h for a load at the tension edge of the beam.

Tables 2 and 3 presents the main dimensions of each of the beams subjected to testing, indicating the initial imperfection for each of them. The given value of imperfection corresponds to the initial transverse displacement at the mid-span of the beams relative to the line connecting the supports at the neutral axis height. Furthermore, measurement of the imperfection at other points of the beam using horizontal transducers (Fig. 7) showed that its shape fits acceptably to a sinusoidal arc, approximately.

As observed in Fig. 8, knots in the wood cause deviations in the longitudinal fibers, which can alter the direction of the stress flow and create stress concentration zones. These deviations, along with other natural or manufacturing defects, may contribute to lateral deviations from the straight alignment of the beams, referred to in this article as initial imperfections. These lateral imperfections have a significant influence on the results, as will be shown in the test outcomes. Therefore, to detect the possible influence of knots and fiber deviations, several beams with identical geometries were tested, and to quantify the influence of the initial imperfection, a stress recording was conducted. Furthermore, the initial rotation of the beams around the longitudinal axis was controlled at the beginning of the test to ensure it was effectively zero. However, other authors have made valuable contributions by considering this effect [12].

The set of tested samples had the certification from the Otto Graff Institute, which guarantees the quality for the strength class of the beams as GL-28, in accordance with the processes of the UNE-EN 14080 standard [26].

### 2.2.2. Configuration of test elements

To carry out the tests, steel frames were designed and manufactured to support the beam at both ends on fork-type supports. This setup simulated the boundary conditions of classical theory were simulated, allowing bending in both planes while preventing warping and torsion about the piece's axis. To avoid anchorage, neoprene was placed on the three faces in contact with the beam, allowing for rotation. The test conditions used for this research can be seen in Fig. 9.

### 2.2.3. Load application system design

To avoid the limitations of the loading methods described in *Introduction*, it was necessary to design a specific load application system for this research. This system aimed to address the issues found in more recent studies [9,12], that is, to allow for free transverse displacement and avoid introducing a horizontal force at the head of the beams. The system developed for this research (Fig. 10) successfully combines the desired aspects of older studies, such as verticality of the load and absence of friction forces at the head of the beams. It also incorporates elements from more modern studies, including continuous load application and real-time data reading with very small-time intervals.

The developed system (Fig. 11) consists, first, of a hydraulic cylinder, followed by a specific coupler for the designed loading apparatus. After this, a fuse is placed as a safety measure, then another coupler is mounted, with the load cell and the frame added next. This frame contains the transverse displacement carriage (Fig. 12), which consists of

**Table 2**

Dimensions of the tested constant depth beams.

Beam N°	Width (mm)	Depth (mm)	Length (mm)	Imperfection
1	77	404	5000	L/1667
2	77	545	6500	L/1300
3				L/2000
4				L/2000
5	76	845	7700	L/513
6				L/770
7				L/1027
8				L/770
9	76	790	8000	L/2000
10				L/2000

**Table 3**

Dimensions of the tested variable depth beams.

Beam N°	Width (mm)	Smaller depth (mm)	Larger depth (mm)	Length (mm)	Imperfection
11	78	145	600	6500	L/2000
12					L/1400
13					L/1200
14					L/1367



Fig. 7. Horizontal transducers to estimate the shape of the initial imperfection of the beams.

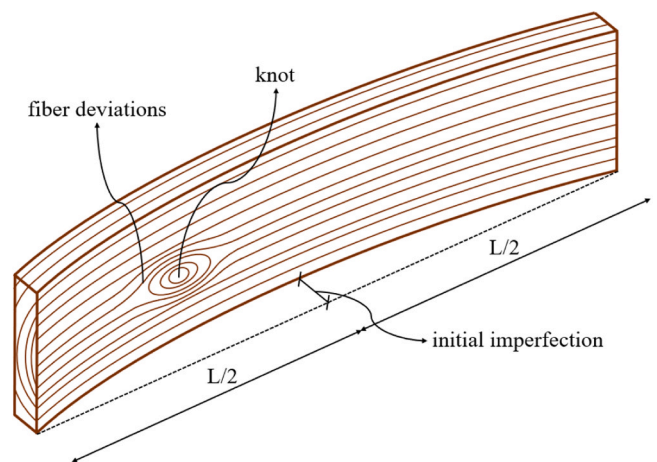


Fig. 8. Knots, fiber deviation and initial imperfection in a wooden beam.

three pairs of bearings, four guides on a side plate, and a load ball joint or ball covered in paraffin. Finally, the ball joint transmits the load to a distribution fork placed on the beam to be tested, which serves as a guide to keep the load application system's movement and the beam's movement in sync.

The designed system allows for a synchronized movement between the load application and the transverse deformation of the beam throughout the entire test. The developed loading system prevents the introduction of loads at the top of the beam, which is crucial for obtaining accurate results, as these horizontal forces at the top can generate torsional moments at the center of the beam, altering the

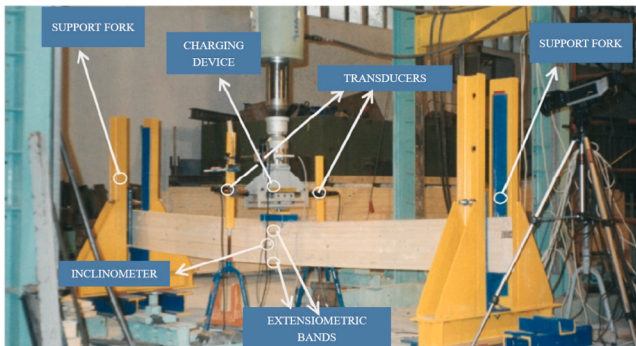


Fig. 9. Laboratory materialization of the indicated component scheme.



Fig. 10. Loading application device.

critical buckling load (Fig. 13). This effect has been avoided through the combination of the lateral displacement carriage, the ball joint, and the distribution fork. Although the friction coefficient at the interface of the loading ball and the distribution plate corresponds to that of two steel elements ( $\mu = 0.2$ ), the small contact surface between them and its lubrication make the friction forces negligible in practice. The load cell and the other instrumentation in place enable continuous data readings.

#### 2.2.4. Instrumentation

The test designed for the research was equipped with instrumentation consisting of a load cell, displacement transducers and strain gauges, in order to provide the applied load at each moment, continuous and simultaneous readings of the transverse displacement and the stress of certain fibers, respectively (Fig. 14).

The strain gauges allow for the quantification of deformations and, therefore, the stresses in the section at the center of the span caused by both longitudinal and transverse displacements, in both tension and compression. Regarding the constant depth beams, six gauges were placed along the fiber direction, paired on each side of the beam's depth: one pair on the most tensioned outer fiber, another pair on the most compressed fiber and the remaining pair within the compressed head (Fig. 15.a).

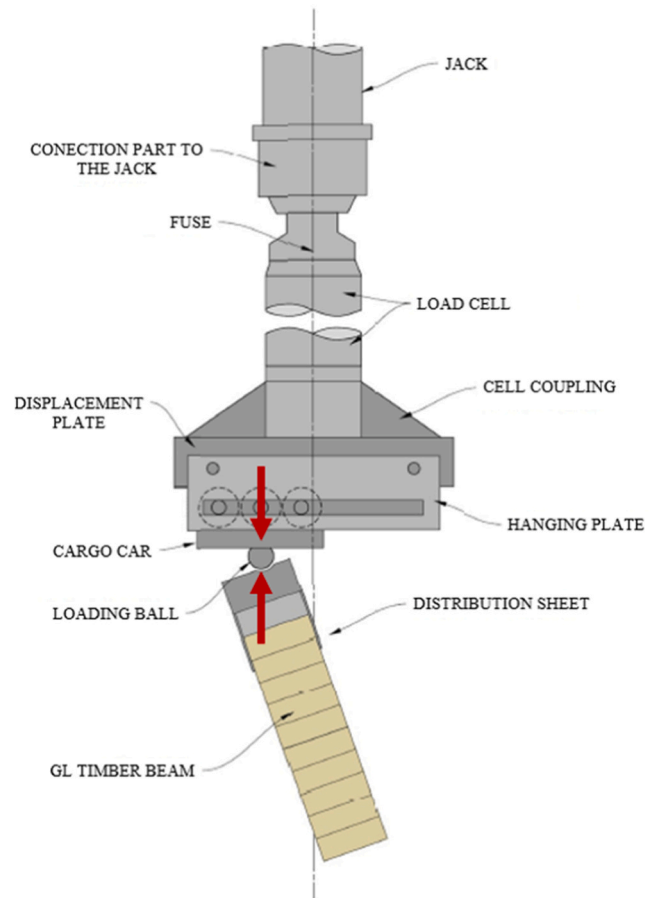


Fig. 11. Components of the loading application system.

For the variable-depth beams, eight gauges were arranged in pairs on each side of the depth, but in this case, some were placed in directions different from the fibers to capture the effect of the varying depth (Fig. 15.b). To control the transverse displacements, two horizontal transducers were used, placed in the center of the span. One was located on each side of the loading car (its movement is equivalent to that of the upper head of the beams), since it is not possible to initially determine in which direction the lateral displacement will occur.

#### 2.2.5. Test system calibration

Before testing the beams, the setup of the testing system was carried out, including the calibration of the loading device, the measurement systems and the support systems, as well as the validation of the testing methodology by comparing the results with classical theory. To complete this task, around thirty planks (Fig. 16) were tested, as the behavior of these specimens aligns better with theoretical expectations, being more homogeneous than the beams, since they consist of a single piece of continuous material rather than a set of laminated layers bonded by adhesive.

In all cases, a good correlation was observed between the experimental results and the theoretical behavior, with a very linear response up to the bifurcation load. This one was generally quite close to the theoretical value for the same slenderness of the tested planks, validating the designed experiment and auxiliary elements as suitable for testing larger laminated wood specimens.

#### 2.2.6. Test results

Next, the results obtained from the instrumentation placed on the strain gauges of the most extreme fiber on the compressed head (the fiber most influenced by lateral instability), on both sides of the cross-

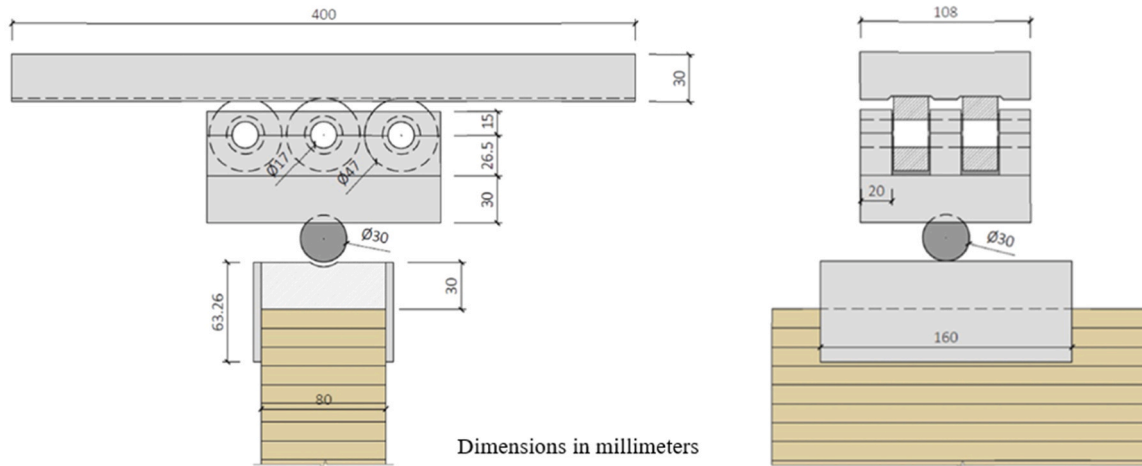


Fig. 12. Cross-section (left) and longitudinal elevation (right) of the transverse displacement carriage with the dimensions of its components.

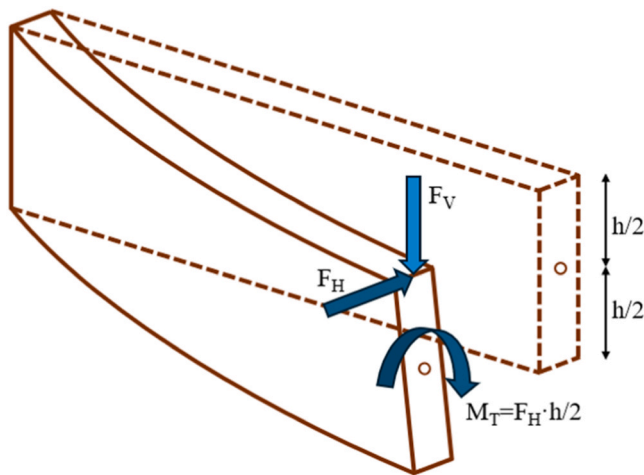


Fig. 13. Internal forces in the cross-section as a consequence of the presence of friction forces at the head of the beam.

section, for the tested GLULAM beams, are presented. These curves (beam load - longitudinal stress in the compressed head) can be seen in the graphs shown in Figs. 17–30, which display the evolution of the stresses on both sides of the cross-section in the tested beams for each load value. Continuous data collection allows for the extraction of the necessary values for the result analysis, such as identifying the load at which the maximum allowed stress for these beams is reached, i.e., the stress  $f_{m,k}$ , which for this case is 28 MPa. In the graphs, on one hand, the horizontal asymptote of the experimental stresses marks the

experimental instability load ( $P_{cu}$ ), and on the other hand, the maximum load at which the beam reaches the maximum allowable stress in bending ( $f_{m,k}$ ), known as the load  $P_{fm,k}$ , is shown for the established initial imperfection level. Also, the load predicted by the EC5 [1] for each test is displayed.

Based on the readings from the horizontal transducers, a graph has been created showing the relative load curves versus transverse displacement for the beams with constant depth (Fig. 31) and variable depth (Fig. 32). The dashed line indicates the inelastic range, while the solid line indicates the elastic range. It is clearly observed that as the initial imperfection increases, the curve's disproportion grows, meaning the second-order nonlinear effects are accentuated. Additionally, it is evident that the value of  $P_{fm,k}/P_{cu}$  decrease for increasing imperfections, that is, the maximum allowable stress in bending is reached for a load less than the asymptotic lateral buckling load.

In the case of the constant depth beams, they beams were intended to be moved until reaching a transverse displacement of 25 cm. However, there were two beams that had not reached the tension  $f_{m,k}$  for this movement, so they continued to be loaded until their displacement was 30 cm. For their part, the variable depth beams were all tested until the measured transverse displacement reached a value of 20 cm.

Finally, images taken during the tests are shown, in which the occurrence of the lateral buckling phenomenon can be clearly seen (Fig. 33).

### 2.3. Numerical analysis

Frequently, instability analyses in wooden structures go beyond the basic calculation cases identified in regulations. In general, real geometries are more complex, boundary conditions are not covered in the

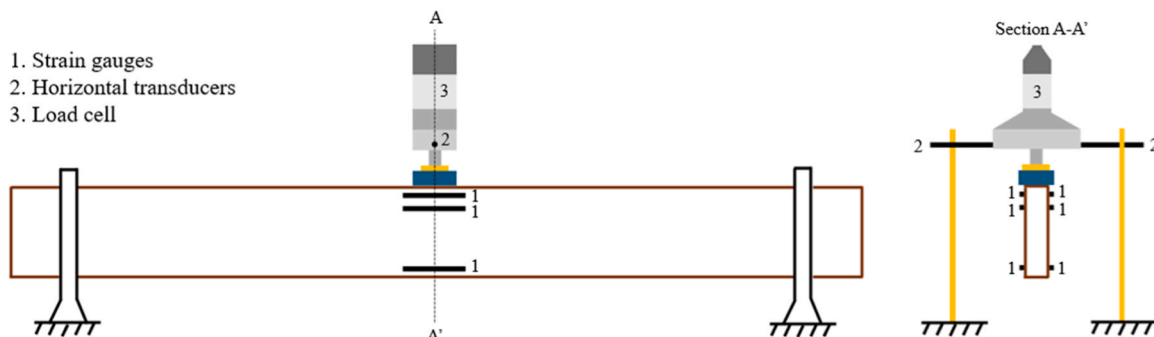


Fig. 14. Constant depth beam with its instrumentation.



a. Extensometric bands on a constant depth beam.

b. Extensometric bands on a variable depth beam.

Fig. 15. a. Extensometric bands on a constant depth beam. b. Extensometric bands on a variable depth beam.



Fig. 16. Carrying out a test on a board.

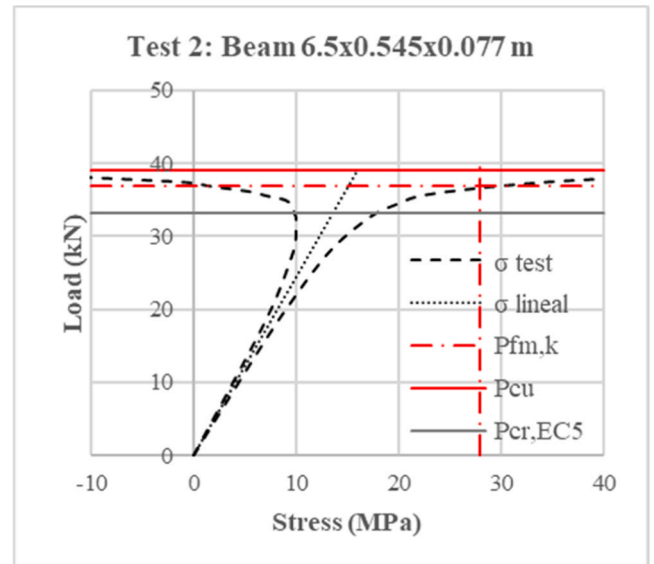


Fig. 18. Graph of results for beam 2.

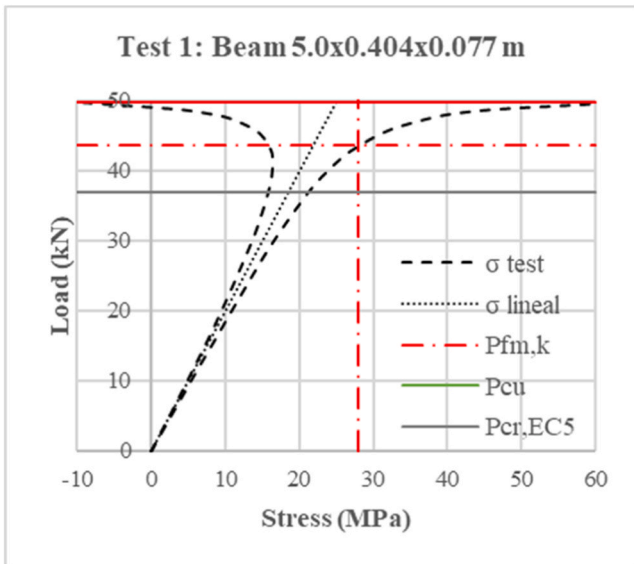


Fig. 17. Graph of results for beam 1.

normative case studies, etc. Many real cases, therefore, require numerical analyses to obtain the critical lateral buckling load values. For this reason, the experimental cases previously described have been modeled, accurately reproducing their testing conditions (geometry, wood mechanical properties, initial imperfections, etc.) using a commercial finite element software (Sofistik). The goal is to validate the numerical analysis by comparing it with Eurocode results under the same conditions, so

that the model can be used with greater confidence in more complex cases where theoretical calculations are not available. Comparison with experimental tests also contributes in this regard.

Both constant and variable depth beams have been modeled as shell elements (Figs. 34 and 35). They have been assigned a GL-28 material with the physical and mechanical properties associated with it according to the UNE-EN 14080 standard [26], a rectangular cross-section, and forked supports at the ends.

To model the forked supports, the three movements were restricted at one of the lower corners of the plate, the vertical and transversal movements at the other lower corner, and only the transversal movement at the upper corners, thus preventing any torsional rotation at the extreme sections. The selected mesh size was 0.10 m, and a sensitivity analysis was conducted to ensure there was no influence from the mesh size. The convergence criterion used was to interrupt the iterative process once the maximum residual force was less than a tolerance equal to one-thousandth of the load. Once the model was set up as detailed, a nonlinear geometric analysis was carried out, through which the load at which structural failure occurs in each beam was obtained.

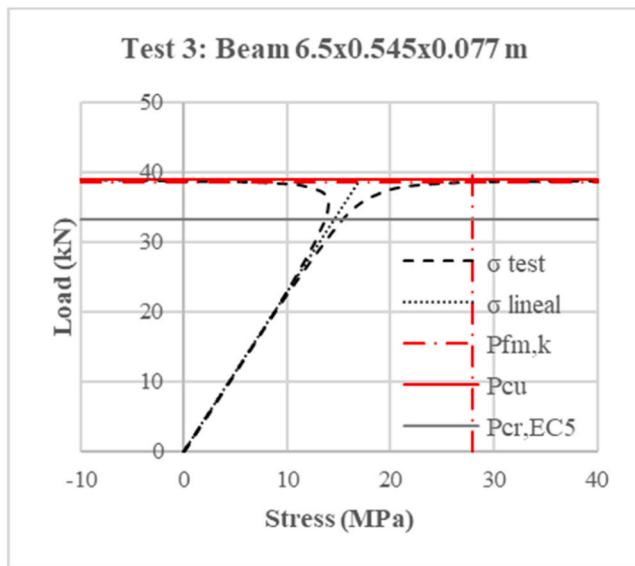


Fig. 19. Graph of results for beam 3.

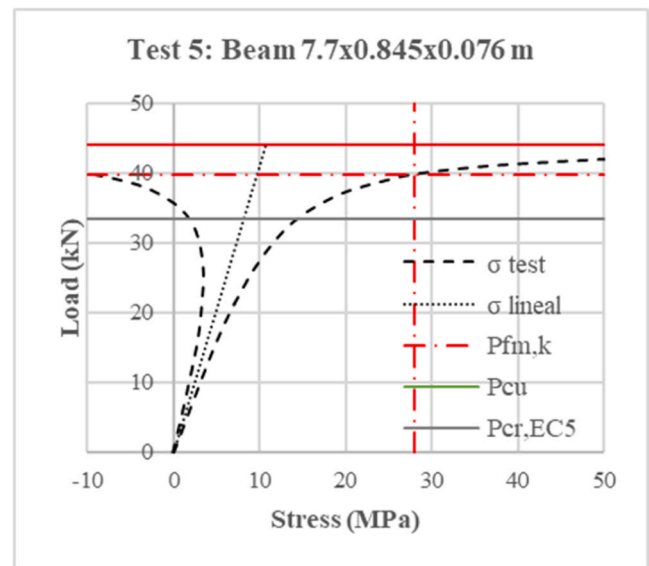


Fig. 21. Graph of results for beam 5.

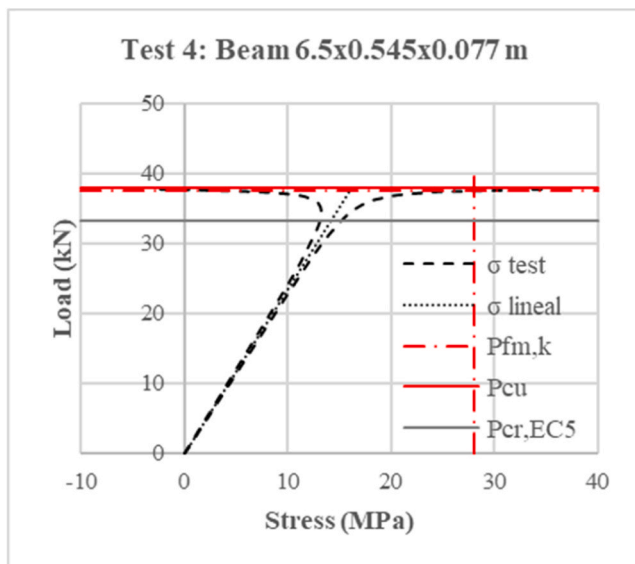


Fig. 20. Graph of results for beam 4.

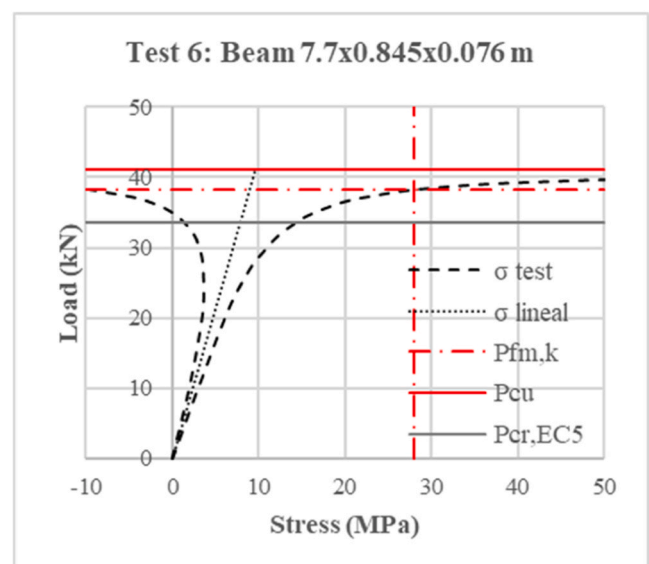


Fig. 22. Graph of results for beam 6.

### 3. Results comparison

Tables 4.1 and 5.1 present the most important results from the three methodologies used, as well as the safety factor provided by the EC5 [1] in relation to the experimental tension failure load obtained, and finally, the relative error measured between each study method considered. For the EC5 [1] calculations, the nominal characteristic values of modulus of elasticity ( $E_{k,UNE-EN\ 14080}$ ) defined in UNE-EN 14080 [26] were used in Eq. [1] and Eq. [2] to obtain  $P_{cr,EC5}$ . Also, that characteristic modulus of elasticity was used in the finite element model to obtain  $P_{cr,FEM}$  through a nonlinear analysis. To further explore the field of safety coefficients, and given that the mean value of the modulus of elasticity ( $E_{mean,UNE-EN\ 14080}$ ) is also defined in UNE-EN 14080 [26], the calculations were repeated to obtain the results for both EC5 [1] and FEM.

Tables 4.2 and 5.2 show these results, allowing for a comparison between the situations resulting from using characteristic and mean values of density ( $\rho$ ) and modulus of elasticity ( $E$ ) in the EC5 [1] formulation and in FEM. These values of the modulus of elasticity

according to UNE-EN 14080 [26] used for the calculations, as well as the modulus of elasticity obtained indirectly from the tests, will be shown in Table 7 in the discussion section.

As shown in Table 4.1, which includes characteristic values of  $\rho$  and  $E$ , the lowest lateral buckling capacity among the three analyzed methods is that of EC5 [1]. This is followed by the value provided by the FEM results, while the highest capacity is observed in the experimental study. This trend is consistent in all cases except for beam 7 and beam 14, the only cases with safety factors lower than one. The result for beam 7 can be considered an anomalous value, as the other three beams with similar characteristics (beams 5, 6, and 8) follow the described order. Similarly, the result for beam 14 is far from the results given by the other three beams with the same characteristics (beams 11, 12, and 13). These significant differences in identical beams show the influence of knots, fiber direction variations, etc.

In the case of the results obtained considering the average values of  $\rho$  and  $E$ , shown in Table 4.2, there is no clear trend where the EC5 [1] provides the lowest value among the three methods. This is consistent

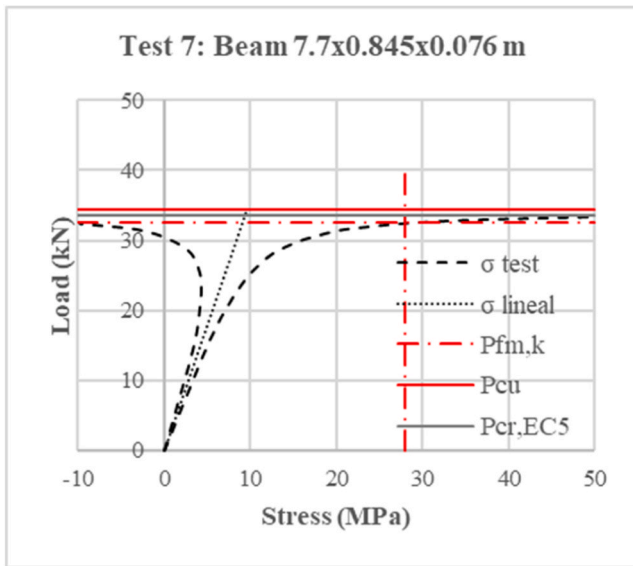


Fig. 23. Graph of results for beam 7.

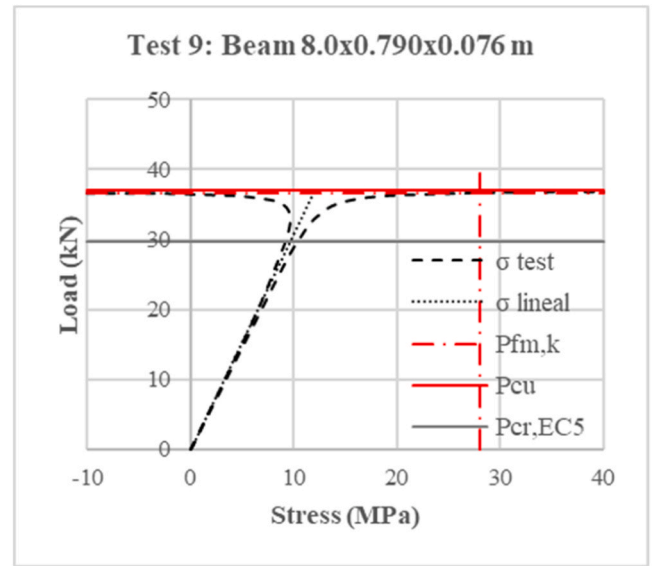


Fig. 25. Graph of results for beam 9.

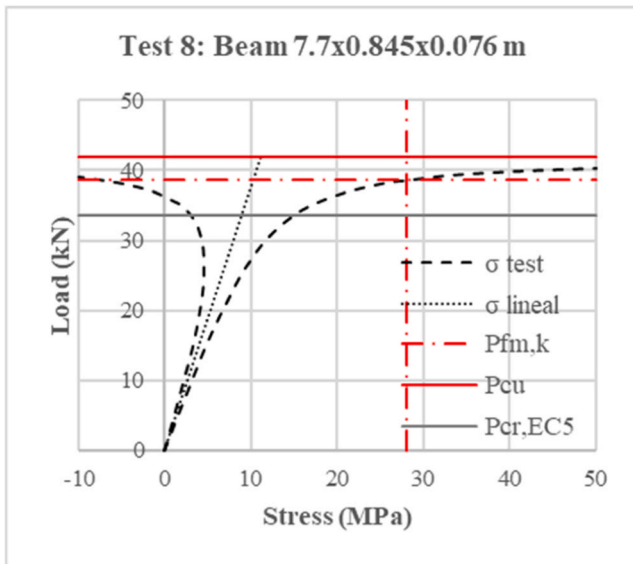


Fig. 24. Graph of results for beam 8.

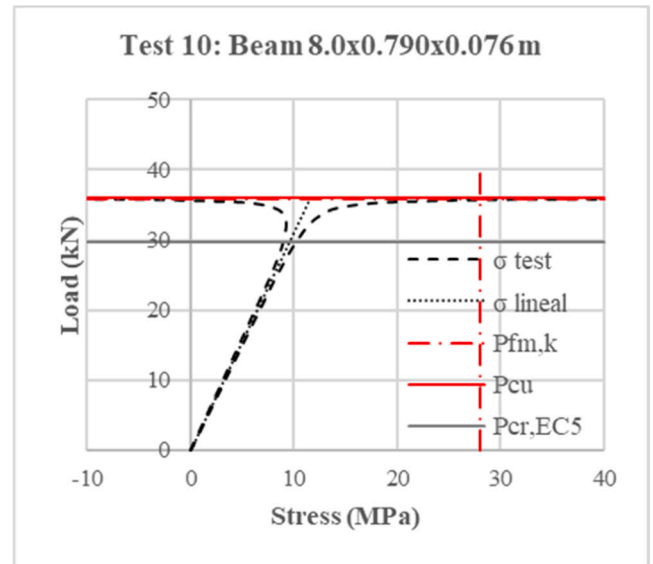


Fig. 26. Graph of results for beam 10.

with the fact that the percentile used for the characteristic values in EC5 [1] determines that in most cases (95 %), the beams should resist more, while with the average values, only 50 % of the tests should resist more. By observing Tables 5.1 and 5.2, it can be seen that the average safety factor approaches 1 when moving from characteristic to average parameters, with values both above and below one. Lastly, based on the error results ( $P_{fm,k} - P_{cr,EC5}$ ) from Table 4.1, it is important to highlight a notable difference in accuracy. The lateral buckling calculations using EC5 [1] for variable-depth beams, treated as if they had a constant depth with their average value (beams 11–14), show a higher error compared to truly constant-depth beams (beams 1–10). On average, this error is about 40 % greater. For this reason, it would be desirable to include the effect of variable depth in the EC5 [1] formulation, given the prevalence of such beams today.

#### 4. Discussion

The formulation of EC5 [1] for studying instability in wood covers

fewer cases of imperfections than those addressed for steel in EC3 [2]. From a professional application perspective, it would be interesting for EC5 [1] to consider additional effects, such as more boundary or load conditions, curved or variable-depth pieces, imperfections, and fiber directions, etc. Currently, EC5 [1] only limits its application to ensuring compliance with a maximum tolerance of  $L/500$  for the initial deviation from straightness at the center of the span (lateral pre-camber). Given the current situation, one of the objectives of this research is to quantify the difference between the behavior of the ideal piece calculated according to EC5 [1] and the real piece, represented by the tested beams. The real behavior of the piece involves transverse deformations before reaching the critical load, i.e., additional second-order stresses appear due to the lateral displacement generated by the nonlinear behavior (second-order nonlinear) before reaching the collapse resistance due to instability. This difference between the linear second-order behavior considered by EC5 [1] and the nonlinear second-order behavior present in the tested beams leads to the failure criterion being reached (a stress of 28 MPa is achieved) at loads lower than the lateral buckling critical

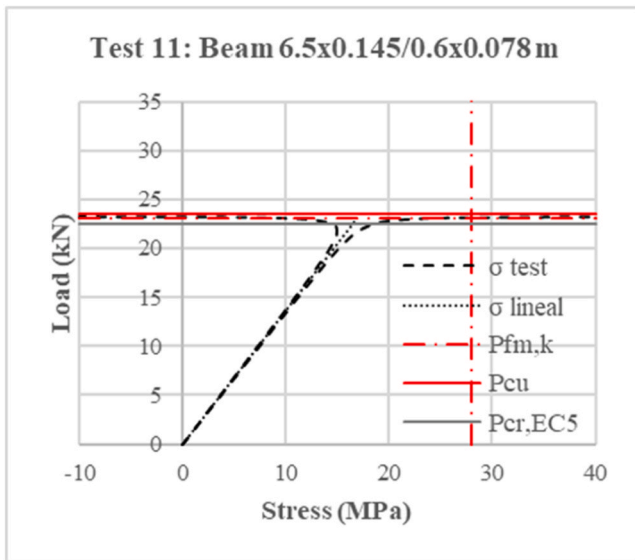


Fig. 27. Graph of results for beam 11.

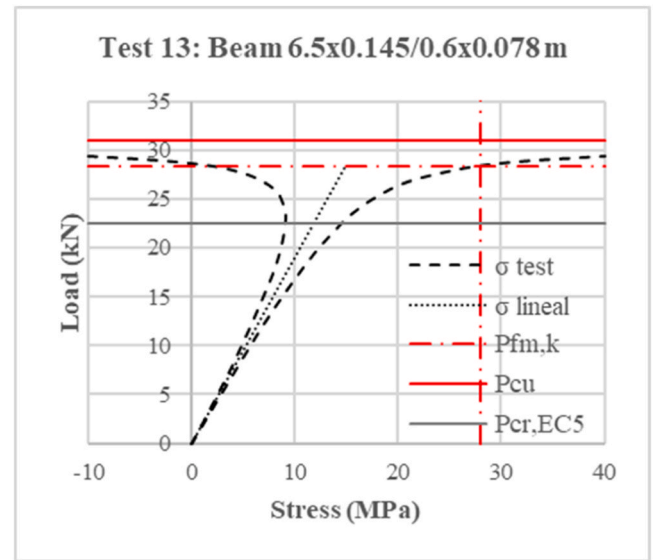


Fig. 29. Graph of results for beam 13.

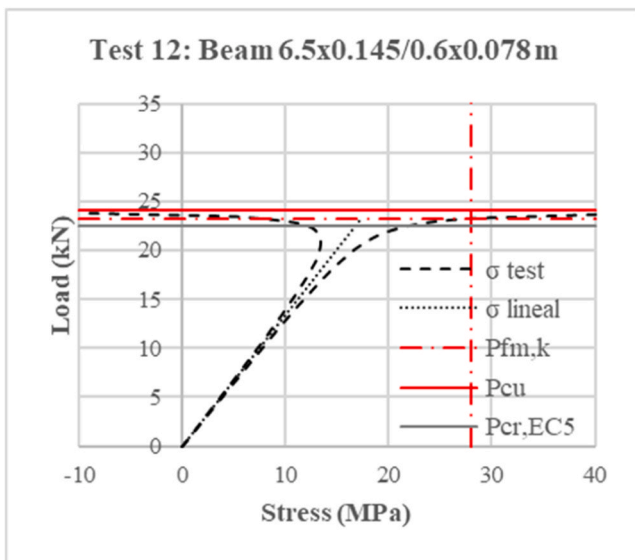


Fig. 28. Graph of results for beam 12.

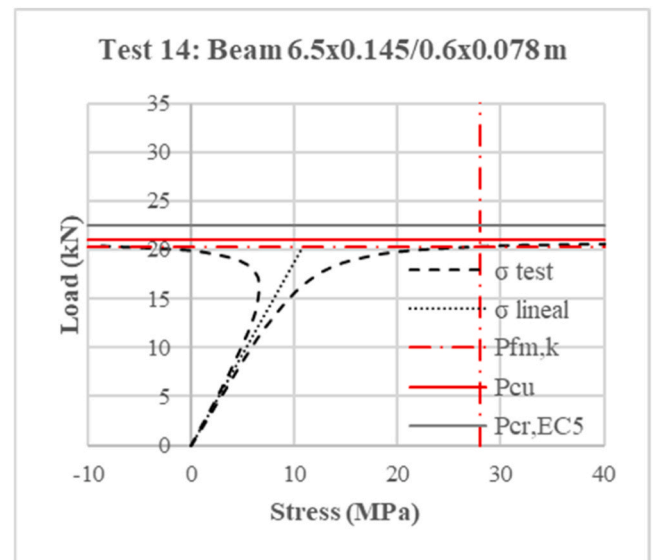


Fig. 30. Graph of results for beam 14.

load, i.e., the stress exhaustion occurs before instability (Fig. 36). Therefore, the failure of the beam due to reaching the limit stress can occur at values lower than the critical load ( $P_{fm,k} < P_{cu}$ ), which are highly influenced by the initial imperfection, as it amplifies the transverse movement and, consequently, the stresses.

To account for the loss of capacity in a simple manner applicable to the professional world, it is proposed to modify the EC5 [1] formulation by introducing a coefficient ( $\omega$ ) that considers this stress limitation. This coefficient will consider the initial imperfection, as the more initial formation there is, the sooner the maximum stress will be reached due to nonlinear effects. The EC5 [1] formulation would be modified as follows

$$R_k \leq \omega k_{crit} f_{m,k}$$

This method of reducing the structure's capacity allows for a linear analysis of the structure to be carried out, directly obtaining the effects of the forces without the need for a nonlinear calculation. Therefore, the goal is to obtain the value of  $\omega$  from the tests, ( $\omega = \frac{P_{fm,k}}{P_{cu}}$ ), which, taking into account the nonlinear behavior, allows for the continued

application of the EC5 [1] methodology with greater confidence. (Note that if the  $\omega$  parameter had been included in the Eurocode calculations in Table 4.1, the safety factor for beam 7 would also have been  $>1$ ). Table 6 summarizes the relative slenderness of the tested beams, the value of the  $k_{crit}$  parameter according to EC5 [1], the  $\omega$  coefficient obtained from the tests, the initial imperfection of each beam, and the range in which each one falls according to EC5 [1] (three ranges based on slenderness: elastic, inelastic, and bending).

Fig. 37 shows the values of the  $k_{crit}$  parameter as a function of the relative slenderness  $\lambda_{rel}$  for the tested beams, in order to categorize them into the three zones defined by EC5 [1].

As can be seen in Fig. 38, there is a very high correlation between the value of the initial imperfection and the factor  $\omega$ . This relationship for the beams tested in the elastic range has an average correlation coefficient ( $R^2 = 0.975$ ). Beam 1 has been excluded from this analysis, although it is shown in the graph, as it falls within the inelastic range. The inelastic range, as previously mentioned, is the area with the greatest difference between theoretical and experimental results due to the straight-line approximation adopted by EC5 [1], so the increase in

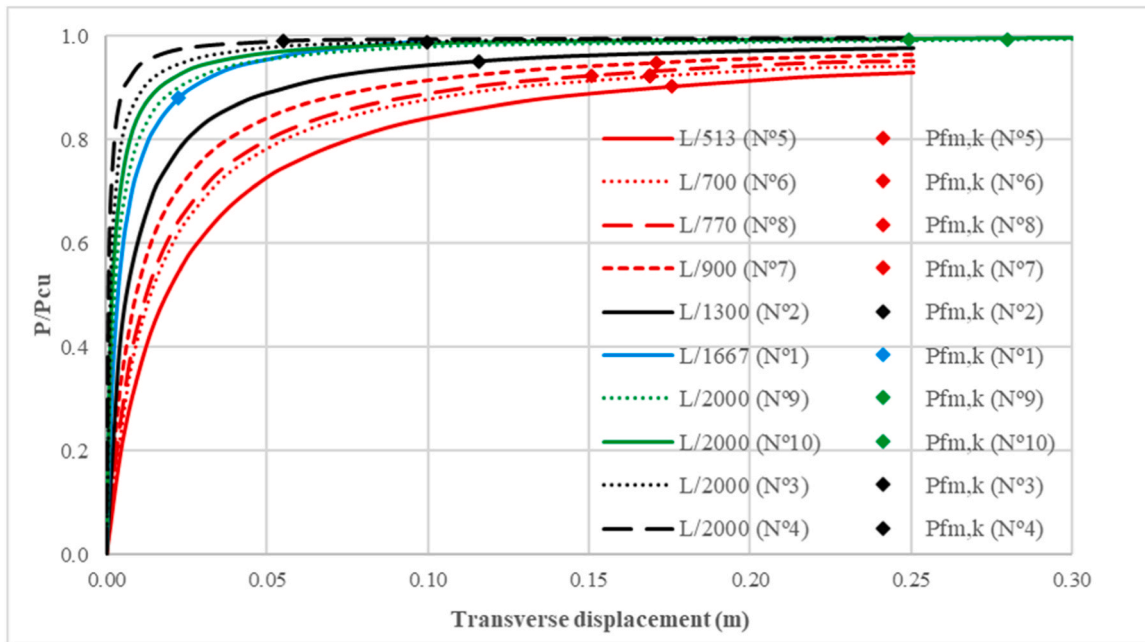


Fig. 31. Relative load vs transverse displacement curves for constant depth beams.

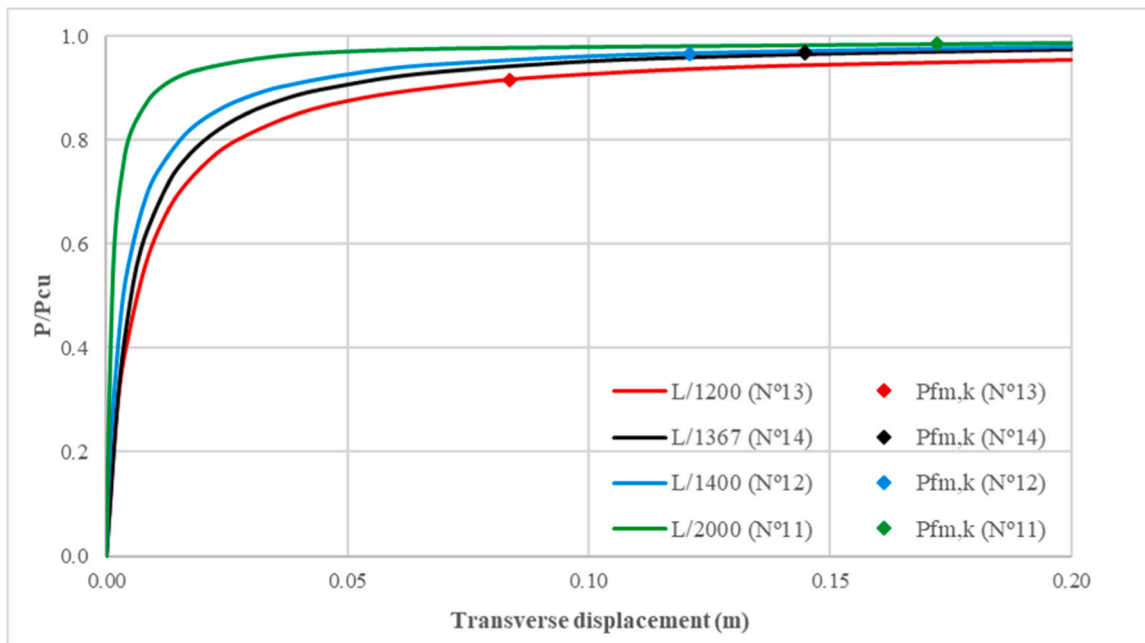


Fig. 32. Relative load vs transverse displacement curves for variable depth beams.

error in the theoretical approximation of this range distorts the influence of the initial imperfection. For this reason, the coefficient is only proposed in the elastic range (the area of greatest influence of lateral instability).

Above all, if the new version of EC5 [1] ultimately modifies the definition of  $k_{crit}$ , as prEN 1995 [24] seems to indicate, may be a review of the proposed factor  $\omega$  presented here will be necessary.

Based on the  $P_{fm,k}$  test results and Eq. [1] and Eq. [2], an indirect measure of the modulus of elasticity in the test was obtained ( $E_{r,test}$ ). That is the equivalent value of elastic modulus needed to obtain the same result as the EC5 [1] calculations and test, assuming the simplification of  $E_k/G_k = 16$ , considered by the standard. These values were then compared with the characteristic and mean value of the modulus of

elasticity according to UNE-EN 14080 [26]. Additionally, although the sample size of the tests is small, the values for the 5 % percentile (characteristic value,  $E_{k,test}$ ) and the 50 % percentile (mean value,  $E_{mean,test}$ ) were obtained, Table 7.

## 5. Conclusions

This research compares the experimental results of lateral buckling tests on full-scale (1:1) glued laminated timber (GLULAM) beams with the values established in the EC5 [1] standard. Additionally, the tests were modeled using finite element software to assess its accuracy and validate its use in analyzing more complex structures, yielding results similar to those of the experimental tests.



a. Lateral buckling deformation I.

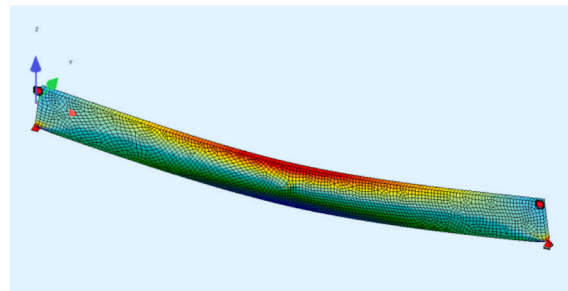


b. Lateral buckling deformation II.

Fig. 33. a. Lateral buckling deformation I. b. Lateral buckling deformation II.

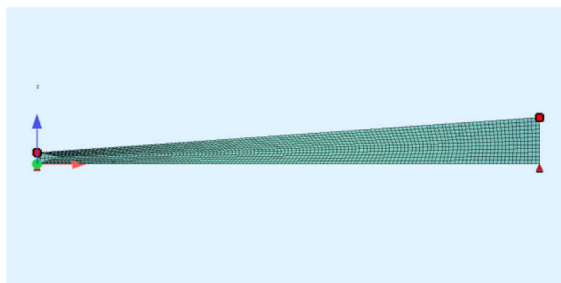


a. Elevation view of the constant depth beam N°2 without deforming (plate type model).

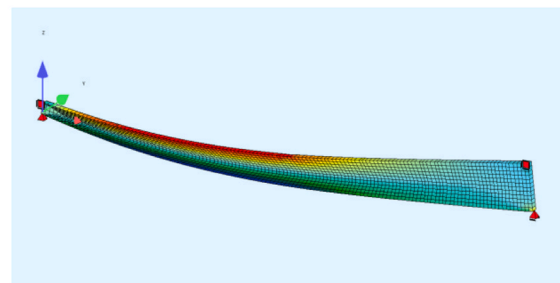


b. Spatial view of the constant depth beam N° 2 deformed (plate type model).

Fig. 34. a. Elevation view of the constant depth beam N°2 without deforming (plate type model). b. Spatial view of the constant depth beam N° 2 deformed (plate type model).



a. Elevation view of the variable depth beams without deforming (plate type model).



b. Spatial view of the variable depth beams deformed (plate type model).

Fig. 35. a. Elevation view of the variable depth beams without deforming (plate type model). b. Spatial view of the variable depth beams deformed (plate type model).

**Table 4.1**  
Main results of each methodology used and comparison between them (characteristic value of  $\rho$  and E).

Depth	N°	Test		$P_{cr,ECS}$ (kN)	$P_{cr,FEM}$ (kN)	Security factor $P_{fm,k} / P_{cr,ECS}$	Error (%)		
		$P_{fm,k}$ (kN)	$P_{cu}$ (kN)				$P_{fm,k} - P_{cr,ECS}$	$P_{fm,k} - P_{cr,FEM}$	$P_{cr,ECS} - P_{cr,FEM}$
Constant	1	43.7	49.7	36.0	43.6	1.22	17.7	0.2	21.4
	2	36.9	39.0	33.2	35.1	1.11	9.9	4.9	5.6
	3	38.5	39.0			1.16	13.7	8.9	
	4	37.6	38.0			1.13	11.6	6.7	
	5	39.7	44.0	33.5	36.1	1.18	15.6	9.0	7.8
	6	38.3	41.2			1.14	12.5	5.6	
	7	32.5	34.3			0.97	3.1	11.2	
	8	38.7	42.0			1.15	13.4	6.6	
	9	36.7	37.0	29.7	31.7	1.24	19.2	13.7	6.8
	10	35.7	36.0			1.20	16.9	11.3	
Variable	11	23.1	23.5	22.5	23.0	1.03	2.6	0.2	2.4
	12	23.2	24.1			1.03	3.2	0.8	
	13	28.2	31.0			1.26	20.3	18.4	
	14	20.3	21.0			0.90	11.0	13.7	

**Table 4.2**  
Main results of each methodology used and comparison between them (mean value of  $\rho$  and E).

Depth	N°	Test		$P_{cr,ECS}$ (kN)	$P_{cr,FEM}$ (kN)	Security factor $P_{fm,k} / P_{cr,ECS}$	Error (%)		
		$P_{fm,k}$ (kN)	$P_{cu}$ (kN)				$P_{fm,k} - P_{cr,ECS}$	$P_{fm,k} - P_{cr,FEM}$	$P_{cr,ECS} - P_{cr,FEM}$
Constant	1	43.7	49.7	39.2	47.2	1.11	10.3	7.9	20.3
	2	36.9	39.0	39.2	37.9	0.94	6.3	2.8	3.3
	3	38.5	39.0			0.98	1.9	1.5	
	4	37.6	38.0			0.96	4.4	0.9	
	5	39.7	44.0	40.2	39.0	0.99	1.3	1.7	2.9
	6	38.3	41.2			0.95	5.0	1.9	
	7	32.5	34.3			0.81	23.7	20.1	
	8	38.7	42.0			0.96	3.9	0.9	
	9	36.7	37.0	35.6	34.3	1.03	3.0	6.7	3.8
	10	35.7	36.0			1.00	0.3	4.1	
Variable	11	23.1	23.5	24.7	25.2	0.93	7.2	9.3	1.9
	12	23.2	24.1			0.94	6.6	8.6	
	13	28.2	31.0			1.14	12.3	10.6	
	14	20.3	21.0			0.82	22.2	2499.5	

**Table 5.1**  
Main statistical parameters of the safety factor (characteristic value of  $\rho$  and E).

Depth	Beams	Maximum security factor	Minimum security factor	Average security factor	Standard deviation of the safety factor
Constant	1	1.22	1.22	1.22	-
	2-4	1.16	1.11	1.13	0.024
	5-8	1.18	0.97	1.11	0.097
	9-10	1.24	1.20	1.22	0.024
	1-10	1.24	0.97	1.15	0.075
Variable	11-14	1.26	0.90	1.05	0.147

**Table 5.2**  
Main statistical parameters of the safety factor (mean value of  $\rho$  and E).

Depth	Beams	Maximum security factor	Minimum security factor	Average security factor	Standard deviation of the safety factor
Constant	1	1.11	1.11	1.11	-
	2-4	0.98	0.94	0.96	0.020
	5-8	0.99	0.81	0.93	0.081
	9-10	1.03	1.00	1.02	0.020
	1-10	1.11	0.81	0.97	0.077
Variable	11-14	1.14	0.82	0.96	0.134

A total of 14 beams, up to 8 m long, were tested: 10 with a constant cross-section and 4 with a variable cross-section, all with an initial imperfection smaller than  $L/500$ . For the tests, an innovative loading

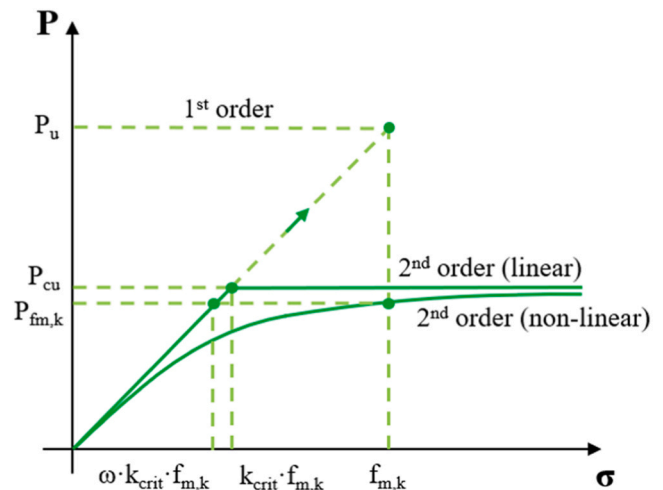


Fig. 36. Ideal behaviour vs Real behaviour.

system was designed to improve precision compared to previous methods. This system featured continuous measurement, vertical load application and the elimination of frictional forces at the load application area.

The experimental results highlight the following considerations:

Two of the 14 beams (beams 7 and 14) exhibited a critical load lower than that predicted by the standard. This deviation was attributed to a higher concentration of knots and fiber deviations in these beams. The

**Table 6**

Parameters that determine the type of lateral buckling for the different constant depth beams.

N°	$\lambda_{rel}$	$k_{crit}$	$\omega$	Imperfection	Range
1	1.074	0.755	0.88	L/1667	Inelastic
2	1.426	0.491	0.95	L/1300	Elastic
3	1.426	0.491	0.99	L/2000	Elastic
4	1.426	0.491	0.99	L/2000	Elastic
5	2.010	0.247	0.90	L/513	Elastic
6	2.010	0.247	0.93	L/770	Elastic
7	2.010	0.247	0.95	L/1027	Elastic
8	2.010	0.247	0.92	L/770	Elastic
9	1.960	0.260	0.99	L/2000	Elastic
10	1.960	0.260	0.99	L/2000	Elastic

lateral buckling critical load varied by 15 % for constant-section beams and 25 % for variable-section beams, even in beams with identical geometry. These findings suggest the need to incorporate the influence of knots into the critical load calculation in the standard, similar to how

geometric imperfections are considered in steel buckling curves. To quantify the influence of knots and fiber deviation on the critical load results for lateral buckling, a larger experimental test campaign would be necessary to obtain accuracy statistics.

All tests included stress measurements to determine whether the maximum bending stress was reached before the critical lateral buckling load. The results demonstrated that the maximum stress increases with larger initial imperfections. The critical load obtained without considering this stress limit (linear second-order analysis) was compared to the critical load accounting for it (nonlinear second-order analysis) to derive a coefficient quantifying the loss of capacity as a function of the initial imperfection. This coefficient, valid within the elastic range defined by the standard, showed a strong correlation ( $R^2 = 0.975$ ). Based on this, a modification to the EC5 [1] formulation is proposed to incorporate this loss of capacity. The tests revealed that an imperfection of L/500 reduces the critical load by 10 %, while imperfections smaller than L/2000 result in a 2 % reduction.

These results should be considered preliminary and require validation through a more extensive experimental campaign to confirm the

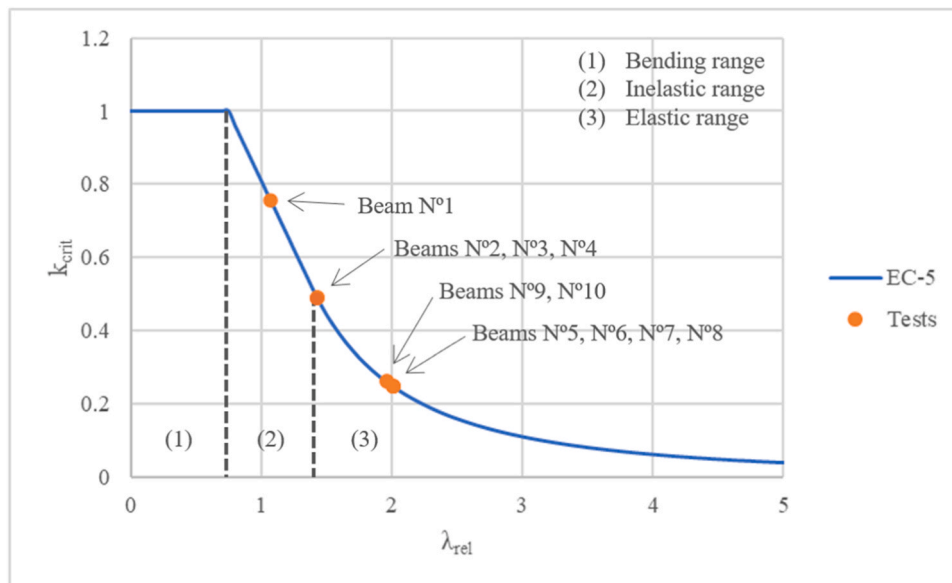


**Fig. 37.** Lateral buckling ranges as a function of slenderness for each of the constant depth beams tested.

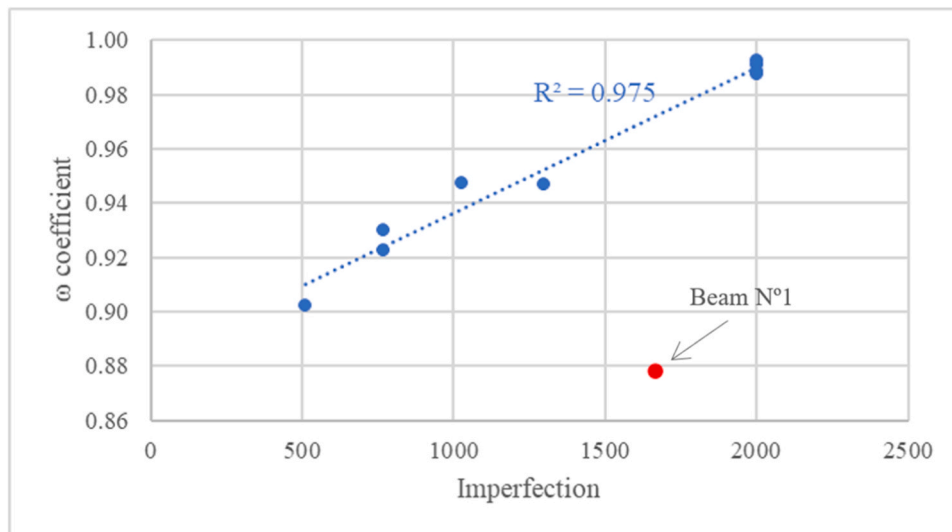


**Fig. 38.** Omega coefficient - imperfection graph.

**Table 7**

Elastic modulus from UNE-EN 14080 [26] and indirect elasticity modulus from tests.

N°	Test $E_r$ (MPa)	UNE-EN 14080	
		$E_{r,test}/E_{k,UNE-EN 14080}$	$E_{r,test}/E_{mean,UNE-EN 14080}$
1	16740	159 %	133 %
2	11660	111 %	93 %
3	12165	116 %	97 %
4	11880	113 %	94 %
5	12440	118 %	99 %
6	12000	114 %	95 %
7	10185	97 %	81 %
8	12130	116 %	96 %
9	12990	124 %	103 %
10	12640	120 %	100 %
11	11015	105 %	87 %
12	11105	106 %	88 %
13	17250	164 %	137 %
14	8935	85 %	71 %
$E_k$ (MPa)	9747.5	10500	
$E_{mean}$ (MPa)	12366.8	12600	

conclusions.

### Declaration of interests

The authors declare that they have no known competing financial interests or personal relationships that could have appeared to influence the work reported in this paper.

### CRedit authorship contribution statement

**Ramos-Gavilán Ana Belen:** Validation, Supervision, Investigation. **Javier Sánchez-Haro:** Writing – review & editing, Writing – original draft, Supervision, Software, Investigation, Formal analysis, Data curation, Conceptualization. **Pablo de Celis:** Writing – original draft, Data curation. **Guillermo Capellán:** Visualization, Validation, Supervision, Resources, Project administration, Methodology, Investigation, Funding acquisition, Formal analysis, Data curation.

### Declaration of Competing Interest

The authors declare that they have no known competing financial interests or personal relationships that could have appeared to influence the work reported in this paper.

### Data availability

Data will be made available on request.

### References

- [1] UNE-EN 1995-1-1:2016. Eurocode 5: Design of timber structures. Part 1-1: General. Common rules and rules for buildings.
- [2] UNE-EN 1993-1-1:2013. Eurocode 3: Design of steel structures. Part 1-1: General rules and rules for building.
- [3] Hooley RF, Madsen B. Lateral stability of glued laminated beams. *J Struct Div ASCE* 1964;90(ST3):201–18. <https://doi.org/10.1061/JSDEAG.0001088>.
- [4] Timoshenko S.P. *Sur la stabilité des systèmes élastiques*. McGraw-Hill (New York), 1953.
- [5] Euler L. *Sur la force des colonnes*. *Mem De l'Acad Des Sci De Berl* 1759;13:252–82.
- [6] Trahair NS. Laterally unsupported beams. *Eng Structures* 1996;18(10):759–68. [https://doi.org/10.1016/0141-0296\(96\)00005-3](https://doi.org/10.1016/0141-0296(96)00005-3).
- [7] Xiao Q, Doudak G, Mohareb M. Numerical and experimental investigation of lateral torsional buckling of wood beams. *Eng Struct* 2017;151:85–92. <https://doi.org/10.1016/j.engstruct.2017.08.020>.
- [8] Larsen HJ. Laterally loaded timber columns: tests and theory. *Int Coun Build* 1977. W18/8-15-1.
- [9] Töpler J, Kuhlmann U. Lateral torsional buckling of glulam beams. 56-12-6 Int Netw Timber Eng Res 2023. <https://doi.org/10.18419/opus-13593>.
- [10] Töpler J, Kuhlmann U, Schänzlin J. Lateral torsional buckling of glulam beam-columns: Axial compression and bending verification. 57-2-1. Int Netw Timber Eng Res 2024. <https://doi.org/10.18419/opus-14995>.
- [11] Feldmann M., Wilden V. & Hoffmeister B. A mechanically consistent approach for stability verification of timber beams in compression and bending around the strong axis, Part 1 - Derivations | Ein mechanisch konsistenter Ansatz für den Stabilitätsnachweis für Holzträger unter Druck und Biegung um die starke Achse, Teil 1 – Herleitungen. *Construction technology | Bautechnik* 2023;100(S1):19-30. <https://doi.org/10.1002/bate.202200073>.
- [12] Wilden V, Hoffmeister B, Feldmann M. A mechanically consistent approach to the stability analysis of timber beams under compression and bending about the strong axis - part 2: experiments and numerics | ein mechanisch konsistenter ansatz für den stabilitätsnachweis für holzträger unter druck und biegung um die starke achse – teil 2: versuche und numerik. *Constr Technol | Bautech* 2024. <https://doi.org/10.1002/bate.202400020>.
- [13] Pelletier B, Doudak G. Investigation of the lateral-torsional buckling behaviour of engineered wood I-joists with varying end conditions. *Eng Struct* 2019;187:329–40. <https://doi.org/10.1016/j.engstruct.2019.03.003>.
- [14] Brünninghoff H, Klapp H. Stability test in wooden constructions: lateral buckling due to torsion with normal force | Stabilitätsnachweis im Holzbau – Biegedrillknicken mit Normalkraft. *Build wood | Bau Mit Holz* 2005;107(10):27–33.
- [15] Hassan OAB. On the structural stability of timber members to Eurocode. *Mech Based Des Struct Mach* 2019;47(5). <https://doi.org/10.1080/15397734.2019.1633344>.
- [16] Töpler J. & Kuhlmann U. Analytical and numerical investigations on imperfection-sensitive timber members subjected to combined bending and axial compression. *World Conference on Timber Engineering* 2021. <https://doi.org/10.18419/opus-12609>.
- [17] Hindman DP, Manbeck HB, Janowiak JJ. Measurement and prediction of lateral torsional buckling loads of composite wood materials: Rectangular sections. *Prod J* 2005;55(9):42–7. 9855.
- [18] Hindman DP, Manbeck HB, Janowiak JJ. Measurement and prediction of lateral torsional buckling loads of composite wood materials: I-joist sections. *Prod J* 2005; 55(10):43–8. 9859.
- [19] Burow JR, Manbeck HB, Janowiak JJ. Lateral stability of composite wood I-joists under concentrated-load bending. *Trans ASABE* 2006;49(6):1867–80. <https://doi.org/10.13031/2013.22289>.
- [20] Jiao P, Borchani W, Soleimani S, McGraw B. Lateral-torsional buckling analysis of wood composite I-beams with sinusoidal corrugated web. *Thin-walled Struct* 2017; 119:72–82. <https://doi.org/10.1016/j.tws.2017.05.025>.
- [21] Ramos-Gavilán A.B. Numerical and experimental study of the flexural behavior of partially embedded beams subjected to high temperatures (Ph. Tesis). University of Salamanca 2015. (<http://hdl.handle.net/10366/128574>).
- [22] Piloto PAG, Ramos-Gavilán AB, Gonçalves C, Mesquita LMR. Numerical and experimental study of bending behaviour of partially encased beams at elevated temperatures. *Fire Saf J* 2017;92:23–41. <https://doi.org/10.1016/j.firesaf.2017.05.014>.
- [23] Argüelles-Álvarez R, Arriaga F, Esteban M, Íñiguez G, Argüelles-Bustillo R. *Estructuras de madera. Bases de cálculo. AsocÓN De InvestÓN Técnica De las Ind De la Madera, Madr* 2013.
- [24] PNE-prEN 1995-1-1:2022. Eurocode 5 (draft version): Design of timber structures. Part 1-1: General rules and rules for buildings.
- [25] Capellán G. Theoretical-experimental study of lateral buckling in glued laminated timber beams (Ph. Tesis). University of Cantabria 2016. (<https://repositorio.unican.es/xmlui/handle/10902/8235>).
- [26] UNE-EN 14080:2022. Timber structures. Glued laminated timber and glued solid timber. Requirements.